Composites Part B 160 (2019) 110–118

Contents lists available at ScienceDirect

Composites Part B

journal homepage: www.elsevier.com/locate/compositesb

Arc erosion behavior of the Al_2O_3-Cu/(W, Cr) electrical contacts

Xiaohui Zhang[a,b], Yi Zhang[a,b,*], Baohong Tian[a,b,**], Junchao An[b,c], Zhuan Zhao[a,b], Alex A. Volinsky[d], Yong Liu[a,b], Kexing Song[a,b]

[a] School of Materials Science and Engineering, Henan University of Science and Technology, Luoyang, 471023, PR China
[b] Collaborative Innovation Center of Nonferrous Metals, Henan Province, Luoyang, 471023, PR China
[c] School of Materials Science and Engineering, Luoyang Institute of Science and Technology, Luoyang, 471023, PR China
[d] Department of Mechanical Engineering, University of South Florida, Tampa, 33620, USA

ARTICLE INFO

Keywords:
Vacuum hot-pressing sintering
Internal oxidation
Electrical contact
Material transfer
Welding force

ABSTRACT

Al_2O_3-Cu/(25)W(5)Cr and Al_2O_3-Cu/(35)W(5)Cr electrical contact materials were fabricated by vacuum hot-pressing sintering and internal oxidation. The relative density, electrical conductivity, and Brinell hardness were measured. The microstructure was analyzed by scanning electron microscopy and transmission electron microscopy. JF04C electrical contact testing apparatus were used to investigate the electrical contact performance of composites. Arc erosion morphologies were analyzed by scanning electron microscopy and three-dimensional profilometer. The material transfer as well as electrical contact performance were studied during contact make and break operations at 30 V DC with current between 10 and 30 A. It indicates that the nano-Al_2O_3 particles pinned dislocations. Material transfers from the cathode to the anode. With the melting, evaporation, and sputtering of Cu during arcing, W particles gather and generate needle-shaped skeletons. Finally, liquid droplets, needle-like structures, craters, and bulges were formed on electrode surfaces after arc erosion. Furthermore, their quantity and morphology are affected by tungsten content. When the content of W in the dispersed copper matrix increases from 25 wt% to 35 wt%, welding force is reduced during the steady operations. In addition, when the arc duration is greater than 8.86 ms, the Al_2O_3-Cu/(35)W(5)Cr contact material has a shorter average arc duration than Al_2O_3-Cu/(25)W(5)Cr at the same arc energy.

1. Introduction

Electrical contacts are widely used in electric power systems, automation, aerospace industry and other fields due to their outstanding electrical contacting properties [1]. These devices play a significant role in connecting circuits, conveying power, and breaking circuits. A variety of physical and chemical erosion processes, including high temperature, welding, wear, and arc discharge take place during initiation, maintenance, and breaking of electric contact [2–4]. As a key component of electrical switches, relays, connectors and circuit breakers, the comprehensive performance of electrical contact material determines the overall performance and service life of electrical switch. According to its function in different situations, some essential requirements of electrical contact material are as follows: outstanding wear and arc erosion resistance, good welding performance, high thermal conductivity and low contact resistance [5].

The compatibility between the secondary phase and the matrix in composite materials can be effectively improved due to the homogeneous microstructures by in-situ reactions. Nano-Al_2O_3 oxide-dispersion-strengthened copper not only has high strength and conductivity, but also high recrystallization temperature and good thermal stability. Due to the strong pinning effects on the grain boundaries and sub-grain boundaries with high dislocation density. Tian et al. [6] have indicated that the Al_2O_3 nano-particles can effectively strengthen the composite. Bera et al. [7] reported that the hardness and wear resistance of the Cu-10Cr-3Ag electrical contact sample increase significantly with the addition of nano-Al_2O_3 particles. Tungsten has a high melting point, high density, high hardness, high strength, and a low thermal expansion coefficient, which result in good arc erosion and welding resistance. Thus, the composite material can be used in electrical contacts. Chromium has good welding resistance, high melting point and strength, small intercepting value, and great affinity to oxygen, which ensures a good inhalation capacity of the contacts. Cu-W and Cu-Cr contact materials have been proved as reliable contact material for vacuum switchgear. Chang et al. [8] found that the average welding force of Cu-Cr-W-C alloys is reduced more than 50% compared

* Corresponding author. School of Materials Science and Engineering, Henan University of Science and Technology, Luoyang, 471023, PR China.
** Corresponding author. School of Materials Science and Engineering, Henan University of Science and Technology, Luoyang, 471023, PR China.
E-mail addresses: zhshgu436@163.com (Y. Zhang), bhtian007@163.com (B. Tian).

https://doi.org/10.1016/j.compositesb.2018.10.040
Received 25 July 2018; Received in revised form 10 September 2018; Accepted 13 October 2018
Available online 15 October 2018
1359-8368/

with the Cu50Cr50 alloy. Yokokura et al. [9] found that CuW has a lower restriking probability than CuCr. Li et al. [10] reported that the addition of W can improve the contact welding resistance of the CuW composite materials. In order to improve welding resistance of the contact material used in medium voltage vacuum interrupters, Nicolle et al. [11] found WCu (10–30% of copper) has much better welding resistance than CuCr (25–50 wt% Cr).

In this paper, Al_2O_3-Cu/(25)W(5)Cr and Al_2O_3-Cu/(35)W(5)Cr contact materials were successfully fabricated by vacuum hot-press sintering and internal oxidation methods. The relative density, electrical conductivity, and Brinell hardness were measured. JF04C electrical contact testing apparatus was used to investigate the electrical contact performance of the composites. The mass transfer and loss mechanisms of different contact materials were studied. The welding force along with the arc duration under different current values was investigated.

2. Experimental

2.1. Samples manufacturing

Cu-0.4Al (Al 0.4 wt%, purity > 99.9%) alloy particles and Cu_2O particles ranging from 2 μm to 5 μm in size were used to prepare Al_2O_3 nano-particle oxide-dispersion-strengthened copper matrix. Cr powder (purity > 99.9%) with an average particle diameter of 44 μm and W powder (purity > 99.9%) with an average particle diameter of 5 μm were used for additional strengthening. Fig. 1 shows the morphology of the different powders characterized by the JSM-5610LV scanning electron microscope. Table 1 shows the composition of Al_2O_3-Cu/(W, Cr). Before sintering in a ZMY-50-15 molybdenum wire vacuum hot-press sintering furnace, powders were adequately mixed in a YH-10 mixer for 2 h using a ball-to-powder weight ratio of 10:1. Copper balls were used as grinding media. The sintering process parameters were 3–4 Pa vacuum, 10 °C/min heating rate, 15 MPa contact pressure applied at 650 °C and held for 1 h, continued by heating to 950 °C held for 1 h, then dropping the temperature to 100 °C prior to sample removal.

2.2. Microstructure characterization

The Sigma2008B1 digital instrument was used to measure the electrical conductivity of as-sintered samples. The relative density was measured and calculated by the Archimedes drainage method using hydrostatic balance. Brinell hardness measurement was carried out with HB-3000B Brinell hardness tester with a load of 2500 N held for 30 s according to the GB/T231.1–2009 standard. Each hardness value is the average of the top and bottom surface measurements. The microstructure of as-sintered samples was analyzed by the JSM-7800F field emission scanning electron microscope and the JEM-2100 transmission electron microscope.

Table 1
Composition of the Al_2O_3-Cu/(W, Cr) composites in wt.%.

Composite	Cu-0.4%Al	Cu_2O	W	Cr
Al_2O_3-Cu/(25)W(5)Cr	66.67	3.33	25	5
Al_2O_3-Cu/(35)W(5)Cr	57.14	2.86	35	5

2.3. Electrical contact testing

As-sintered composites were cut into Φ3.8 mm × 8 mm size cylindrical specimens by wire-electrode cutting machine, and then used as the anode and the cathode electrical contacts. The specimen surfaces were grinded and polished. The specimens were weighed by the FA2004B electronic balance before and after the predetermined operations, with each data point representing the average result of 5 operations. The mass transfer and the loss of the contacts suffering arc erosion, △m, was calculated as follows,

$$\triangle m = m_2 - m_1$$

Here, m_2 is the electrode mass after electrical contact testing and, m_1 is the specimen mass before electrical contact testing.

Ten thousand contact cycles were performed on the JF04C electrical contact testing apparatus, which is shown in Fig. 2. These tests were conducted under the argon atmosphere. The bottom contact was stationary and served as a cathode, while the top contact was movable. The test was carried out in the constant current mode with the voltage set to 30 V DC and the current set to 10, 20, 25, and 30 A. The contact force was 0.4–0.6 N and the contact breaking frequency was 1 Hz. Finally, the specimens were weighed again after the test. Three contact samples were tested in this paper for the repeatability of experimental results. The arc erosion morphology of the contacts was analyzed by the JSM-5610LV scanning electron microscope and the three-dimensional profilometer.

3. Results

3.1. Properties and microstructure

Fig. 1 illustrates the SEM morphology of different kinds of raw

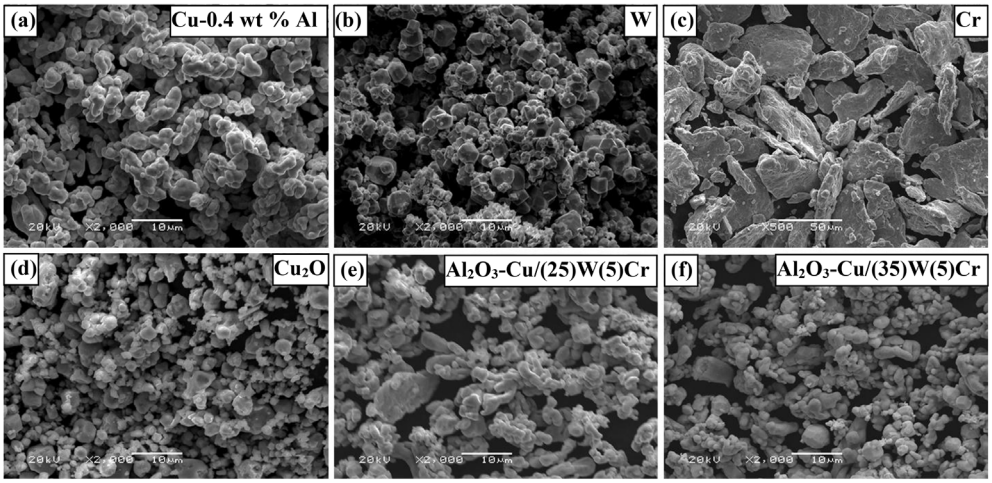

Fig. 1. SEM images of the feedstock powder: (a) Cu-0.4 wt% Al; (b) W; (c) Cr; (d) Cu_2O; (e) mixed powder of Al_2O_3-Cu/(25)W(5)Cr; (f) mixed powder of Al_2O_3-Cu/(35)W(5)Cr.

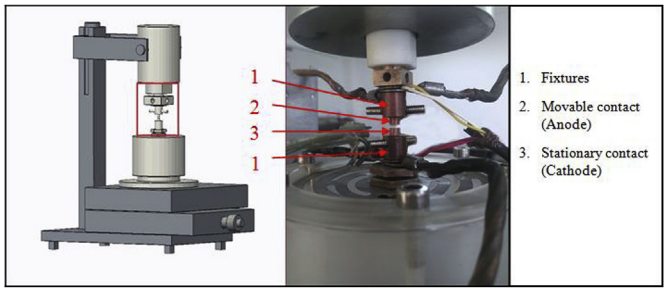

Fig. 2. JF04C electrical contact testing apparatus.

powders used in the Al_2O_3-Cu/(25)W(5)Cr and Al_2O_3-Cu/(35)W(5)Cr composites before and after mixing. It is seen that the powder used in the two composites was mixed homogeneously (Fig. 1(e) and (f)).

Table 2 shows the comprehensive properties of the two kinds of composites. The relative density of the composites was above 97%. When the W content was increased from 25 wt% to 35 wt%, the electrical conductivity of the as-sintered samples decreased from 67.28 % IACS to 62.20 %IACS. However, Brinell hardness increased from 102.31 HBW to 126.78 HBW. The electrical conductivity is one of the most

Table 2
Comprehensive properties of the Al_2O_3-Cu/(W, Cr) composites.

Composite	Relative density, %	Electrical conductivity, %IACS	Brinell hardness, HBW
Al_2O_3-Cu/(25)W(5)Cr	97.25	67.28	102.31
Al_2O_3-Cu/(35)W(5)Cr	97.62	62.2	126.78

significant factors for evaluating the performance of electrical contacts. Electrical properties of composites are affected by the dispersed Cu matrix, which is higher than that of W particles. In addition, W and Cu are incompatible, which increases matrix imperfections. Therefore, the residual porosity in the sintering process and the internal stresses between the added phase particles and the matrix will enhance electron scattering. Furthermore, Brinell hardness is affected by the Al_2O_3 and W nano-particles distributed in the matrix. The pinning effect of Al_2O_3 and W particles causes tangles and intersection of dislocations, obstructing their movement. In addition, the hardness of the composite material increases due to the reaction force of the dislocation ring on the dislocation source caused by dislocation pile-up. This phenomenon can be seen in Fig. 4(d).

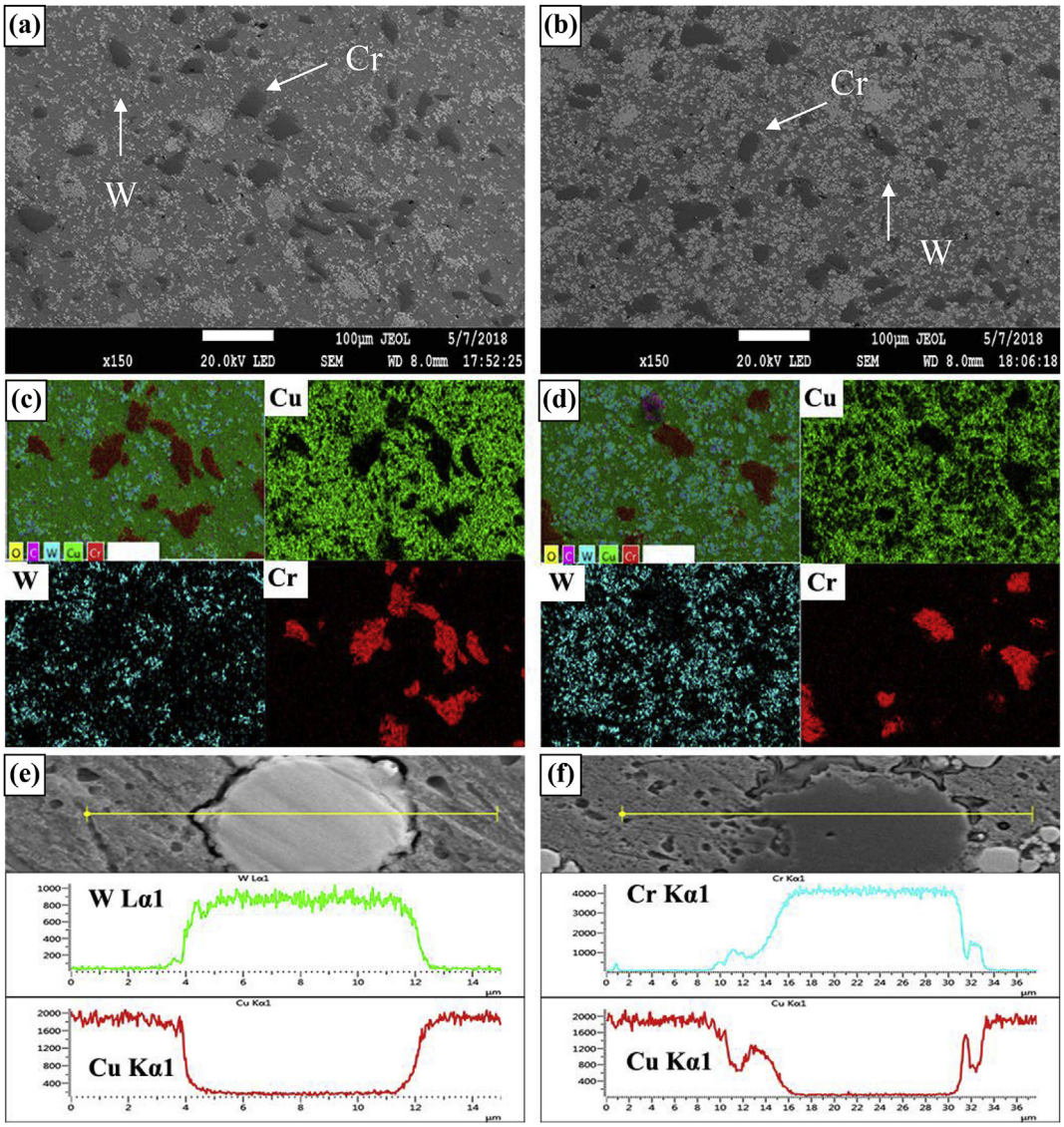

Fig. 3. SEM images, corresponding EDS maps at high magnification and element line scans (a, c ,e) Al_2O_3-Cu/(25)W(5)Cr; (b, d, f) Al_2O_3-Cu/(35)W(5)Cr.

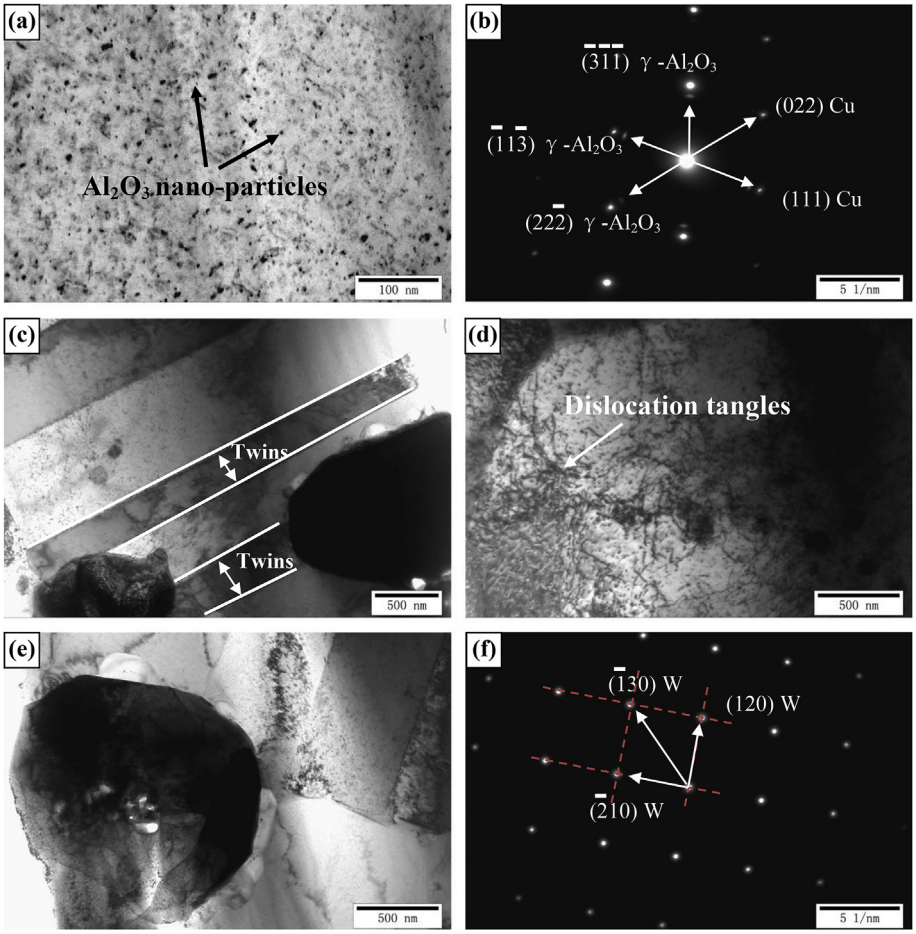

Fig. 4. TEM images of the Al_2O_3-Cu/(35)W(5)Cr composite: (a, c, d, e) HRTEM images; (b, f) Selected area electron diffraction pattern and indexing.

SEM images, low-magnification EDS layered superposition images and corresponding element mapping of two composites, EDS line scans are shown in Fig. 3. As seen in Fig. 3(a) and (b), the two kinds of composites have a compact structure without defects such as pores and particle clumping. W and Cr particles are distributed uniformly in the dispersed copper matrix, where small particles are W and larger particles are Cr. The EDS line scans reveal that there is no mutual solubility between Cu and W, while there is a very narrow transition region between Cr and Cu.

The Al_2O_3-Cu/(35)W(5)Cr composite microstructure, which was analyzed by transmission electron microscopy, is shown in Fig. 4. As seen in Fig. 4(a), a large number of Al_2O_3 nano-particles are distributed in the copper matrix. Fig. 4(d) shows dislocations intersections and tangles caused by the Al_2O_3 nano-particles pinning dislocations. The Orowan strengthening effect contributes to good mechanical properties of the Al_2O_3-Cu/(W, Cr) contact materials. Fig. 4(c) shows orderly distributed twins. It is known that twin boundaries have the same effects as hindering dislocation migration and grain boundaries. Twin boundaries reduce the average movement of dislocations. Thus, they can increase the dislocation density and material hardness [12–15]. These effects also improve the arc erosion resistance of the contact material.

3.2. Material transfer

Due to the arc erosion, the transfer and loss of contact material directly affect the service life of electrical contacts and leads to component failure eventually. When arc erosion takes place, the material is separated from the electrodes by evaporation, liquid spatter or detachment due to the input of the arc heat flux and arc force on the electrode surface.

Fig. 5 shows the mass change of contacts with 30 V DC, 10–30 A. Compared with the results of the first test (Fig. 5(a) and (b)) and the other repeated tests twice (Fig. 5(c) and (d)), different specimens of the same material presented similar mass change trends. Considering the experimental fluctuations and results repeatability, Fig. 5(c) and (d) represent the mass change characteristics better. For the Al_2O_3-Cu/(25)W(5)Cr contacts, the cathode mass loss and the anode mass gain took place from 10 A to 30 A. Two stages can be seen in Fig. 5(c). From 10 A to 25 A, the net transfer rate increased with the current. However, both the anode mass and the cathode mass at 30 A had less change than that at 25 A. For the Al_2O_3-Cu/(35)W(5)Cr contacts in the repeated tests, the cathode mass loss and the anode mass gain took place under all conditions. In addition, the mass change value increased consistently with the current increase from 10 A to 30 A. According to Fig. 5, all the total mass change value were negative, i.e., the anode mass gain was not equal to the cathode mass loss. This indicates a material loss to the environment.

Due to the low current and low temperature of arc column from 10 A to 25 A, less charged particles were produced by collision and thermal ionization. In order to maintain the arc, electrons need to be emitted from the cathode. Positive ions accumulating in the cathode surface area resulted in the higher electric field intensity. At the same time, the arc constriction in the cathode area increased the current density. As a result, more particles near the cathode were ionized. Thus, positive ions accumulated and arc constriction in the cathode area increased the heat flux which was input into the cathode [16]. Consequently, the material transferred from the cathode to the anode. The mass transfer directions

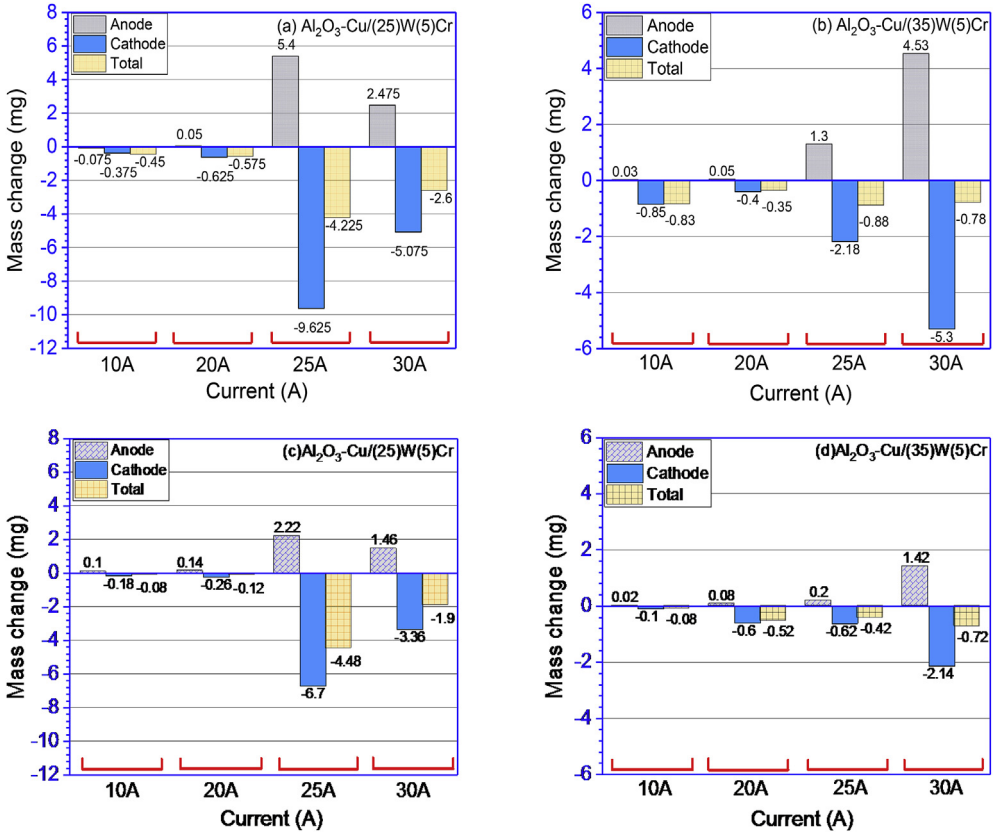

Fig. 5. Mass change after different tests: (a) and (b) the first test; (c) and (d) the repeated tests.

of the Al_2O_3-Cu/(25)W(5)Cr and Al_2O_3-Cu/(35)W(5)Cr contacts were from the cathode to the anode with the current increased from 10 A to 25 A. On the contrary, the number of charged particles at 30 A was more than at 25 A. Maintaining the arc no longer depended on arc constriction in the cathode area and ionization of the electrons which were emitted from the cathode. Then the arc constriction phenomenon in the cathode area disappeared. In order to maintain the arc, the arc column in the anode area constricted. Instantaneous and concentrated heat flux was inputted into the anode contact. Thus the material transferred from the anode to the cathode. Although the material transfer direction changed, the material which transferred from the cathode to the anode predominated the final transfer direction. Hence when the current was set to 30 A, both the anode and cathode mass of the Al_2O_3-Cu/(25)W(5)Cr had less change than that at 25 A.

However, the Al_2O_3-Cu/(35)W(5)Cr contacts have higher tungsten content. Tungsten has a high melting point, low saturated vapor pressure, high latent heat of fusion and vaporization. Thus, the Al_2O_3-Cu/(35)W(5)Cr contacts produced fewer particles due to collision and thermal ionization at 30 A. Maintaining the arc still depended on arc constriction in the cathode area and ionization of the electrons which were emitted from the cathode. Thus, the material cannot transfer from the anode to the cathode. The mass change value increased consistently from 10 A to 30 A.

In order to investigate and explain material transfer in the process of arc discharge, Chen et al. [17] proposed the particle sputtering and deposition (PSD) model. In the model, the discharge ions in the metallic phase and gaseous phase play different roles in the material transfer process. In the metallic phase, the arc takes place in metal vapor, and charged particles are mainly electrons, and metal ions, etc. This causes electron sputtering on the anode and ion deposition on the cathode. Thus, material transfers from the anode to the cathode. In the gaseous phase, the dominant particles include gaseous ions and metal atoms. When the cathode is bombarded by the gaseous ions, sputtering occurs and cathode particles transfer to the anode. Jemaa et al. [18] reported that the transition from an anodic arc stage to a cathodic arc stage takes place at a critical arc length. As a result, arc erosion is caused by the combined action of these stages, in which the dominant process ultimately determines the electrode material transfer direction. When W is added to the dispersed copper matrix, the hard needle-shaped skeleton left after arc erosion can restrict the flow of molten metal. For the Al_2O_3-Cu/(W, Cr) contact materials, the material which transferred from the cathode to anode predominated the final transfer direction.

3.3. Arc erosion morphology

Fig. 6 shows the three-dimensional morphology of the two electrical contacts after arc erosion under 30 V DC, 20 A. Obviously, remarkable changes took place on the surface. The three-dimensional models can contribute to the analysis of the arc erosion process. As seen in Fig. 6, some peaks and craters are formed on the anode and cathode surfaces, respectively.

Fig. 7(a–d) show low-magnification images of the two electrical contacts surfaces after 10000 cycles at 30 V DC, 30 A. It is seen that the contact surfaces of both materials are affected by arc erosion. Many hills and craters are formed on the anode and the cathode surfaces, respectively. It can be seen that the morphology of the cathode in Fig. 7(d) contains a smaller quantity and shallower craters compared with Fig. 7(c). In addition, coral structures and a large bulge can be seen on the anode contact surface in Fig. 7(a), which are not present in Fig. 7(b).

Fig. 8 shows EDS results of the two different as-sintered materials and complete electrode surface after the arc erosion test. For the Al_2O_3-Cu/(25)W(5)Cr anode, Cu content slightly increased after arc erosion, while Cu content of the Al_2O_3-Cu/(35)W(5)Cr contact material slightly decreased. For the cathode, Cu content of both materials significantly decreased, while W content significantly increased. The reason is that

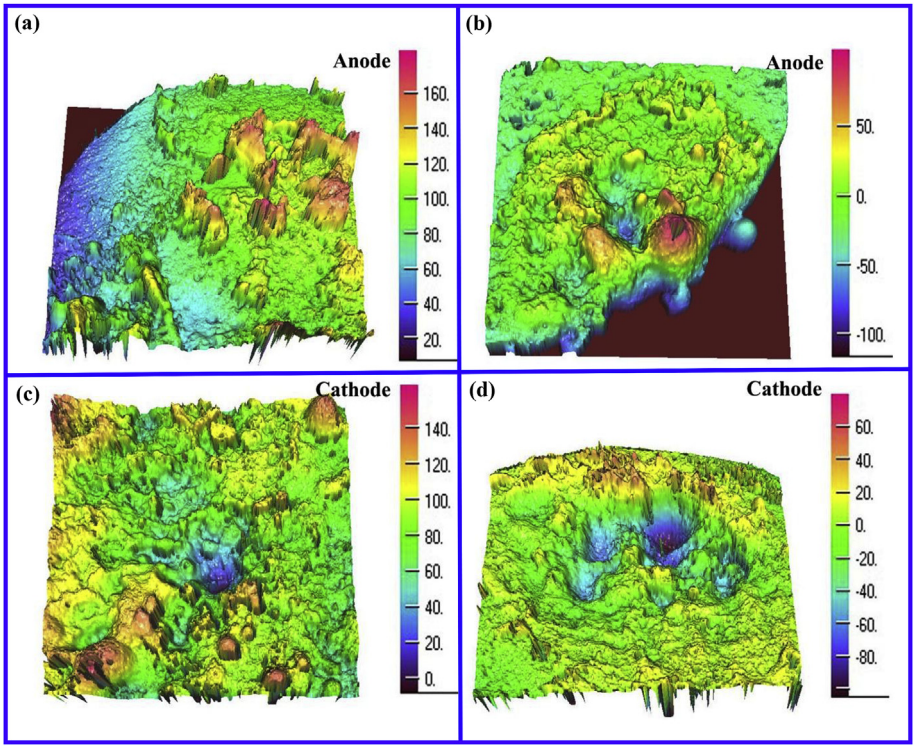

Fig. 6. Three-dimensional morphology of: (a, c) Al_2O_3-Cu/(25)W(5)Cr and (b, d) Al_2O_3-Cu/(35)W(5)Cr at 30 V DC, 20 A. Vertical scale is in μm.

W has higher melting and boiling points, which reduce material evaporation during the arc erosion process compared with Cu. Thus, the rate of material loss of W during arc erosion is lower than that of Cu.

Fig. 9 shows high-magnification images of two materials' contact surfaces after arc erosion at 30V DC, 30 A. Liquid droplets, needle-like structures, craters, and bulges were formed on the electrode surfaces after arc erosion as seen in Fig. 9(a), (b), Fig. 9(c), and Fig. 9(d), respectively. These are typical surface features of arc erosion. Furthermore, a liquid spreading phenomenon took place on the cathode surface, seen in Fig. 9(c) and (d), with many coral structures located nearby in boxed areas 2 and 4. The initial phase of opening contacts produces a molten metal bridge. The arc forms due to the bridge ruptures close to or above its boiling temperature when the contacts continue to open. The high temperature of the electric arc formed during the process of contact separation melts the surface of the contact into a molten pool. Due to the low melting and boiling temperatures, the Cu melts first and spatters, causing material transfer and loss [19,20]. As temperature drops, the material solidifies and forms a spiral

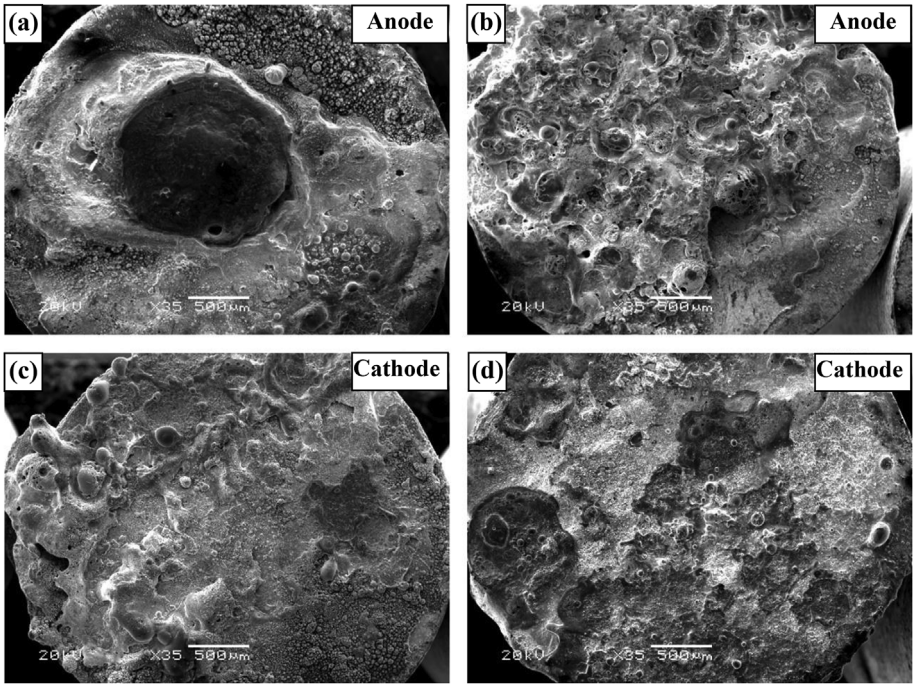

Fig. 7. SEM low magnification images of arc erosion of: (a, c) Al_2O_3-Cu/(25)W(5)Cr and (b, d) Al_2O_3-Cu/(35)W(5)Cr.

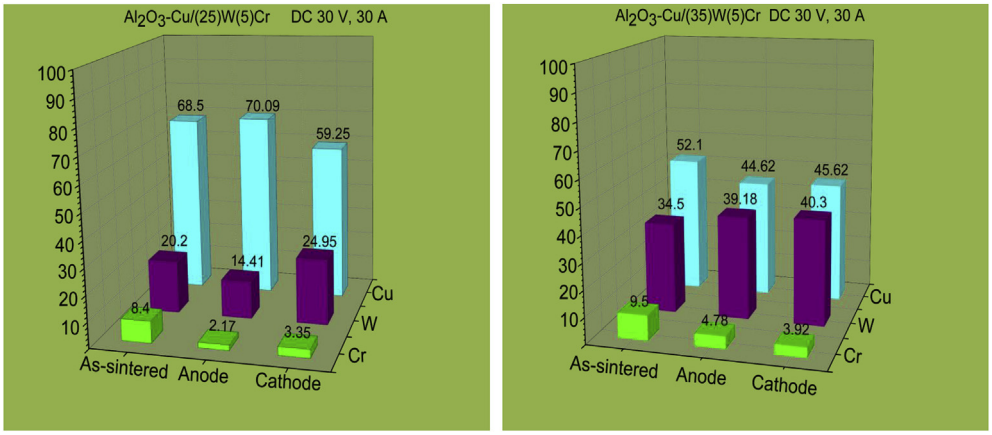

Fig. 8. Element surface analysis of two different as-sintered materials and complete electrode surface after arc erosion tests.

morphology, while W particles gradually gather to form many needle-shaped skeletons. This can be proven by EDS results in Fig. 10.

Fig. 10 shows EDS results of the two different as-sintered samples and four boxed areas from Fig. 9. According to Fig. 10, the Cu content of the area 1 on the anode surface in Fig. 9(a) reached 85.9 wt%, which is much higher than the Cu content in the as-sintered sample. It should be noted that the W content of the area 3 is 70.3 wt%, which is significantly higher than the W content in the as-sintered sample. Areas 2 and 4 contain many coral structures, and EDS data illustrates that the W content in areas 2 and 4 reached 54 wt% and 53.6 wt%, respectively.

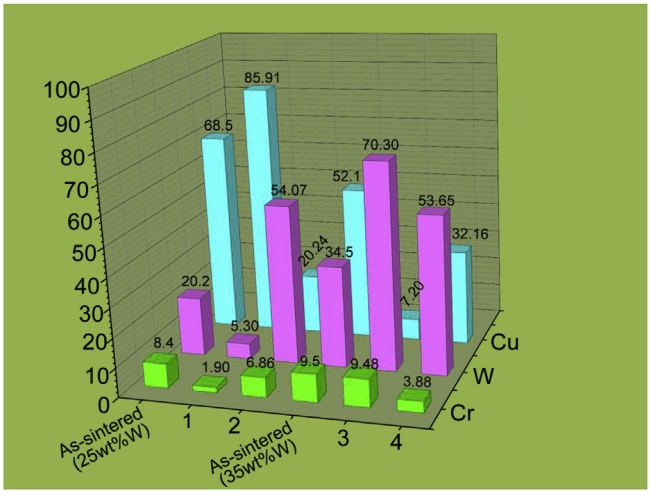

Fig. 10. Elemental surface analysis of two different as-sintered samples and four boxed areas.

4. Discussion

4.1. Welding force

Arcing occurs during making and breaking electrical contact associated with material transfer and welding, which eventually leads to material failure. Laurent et al. [21] had announced that welding occurs at the beginning of the bounce. Arcing causes the contacts' surface to be heated to the melting point. After the arc is extinguished, material

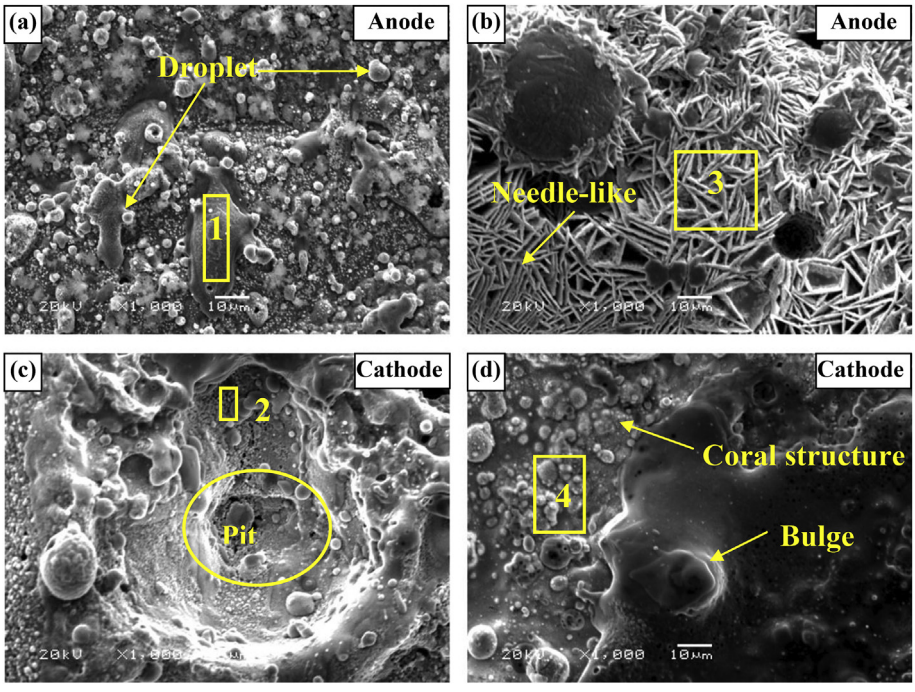

Fig. 9. SEM high magnification images of arc erosion of: (a, c) Al_2O_3-Cu/(25)W(5)Cr and (b, d) Al_2O_3-Cu/(35)W(5)Cr.

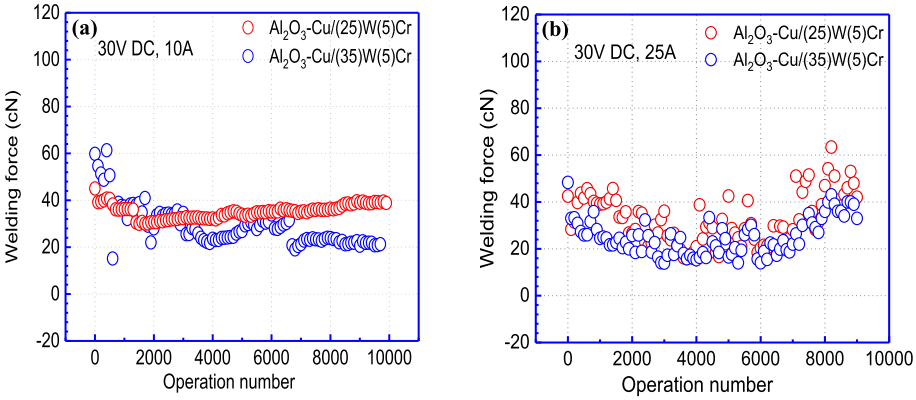

Fig. 11. Relationship between welding force and operation number (a) 30V DC, 10 A; (b) 30V DC, 25 A.

solidification occurs resulting in welding. The research of Yu Li et al. [22] shows that the melting point, latent heat of melting, latent heat of gasification, and heat conductivity of the contact material are positively proportional to welding resistance.

Under the 30 V DC, 10 A and 30 V DC, 25 A test conditions, the welding forces of Al_2O_3-Cu/(25)W(5)Cr and Al_2O_3-Cu/(35)W(5)Cr contact materials, with each data point representing the average result of 100 breaking operations, are shown in Fig. 11. It can be seen from Fig. 11 that as current increases, the average welding force between Al_2O_3-Cu/(25)W(5)Cr and Al_2O_3-Cu/(35)W(5)Cr changes a little, but the fluctuation range gradually increases. Under 30 V DC, 25 A, the average welding forces of the two contact materials are 0.31 N and 0.23 N, respectively. However, in the early stage of testing, the sample with 35 wt% W shows larger welding force than the sample with the 25 wt% W. Electrodes contact conditions were different due to different original morphology, surface roughness and the position of the contact surface in the early stage of testing. Specifically, the surface roughness has the greatest effect on the welding force. Thus, the fluctuation of the welding force took place in the early stage. When the W content in copper matrix composites increased from 25 wt% to 35 wt%, the welding resistance improved. Since W and Cu cannot form a solid solution, a large number of dispersed hard W particles form a needle-shaped skeleton structure in the welding zone, which has a large weakening effect on welding.

Based on the welding tendency and welding force of different materials, Liu et al. [23] established a one-dimensional evaluation mode expressed by the following equations:

$$k_w = \frac{\varphi_e T_m \sqrt{C\rho\lambda}}{\varphi_i^2 \varphi_a} \tag{1}$$

$$F = k(0.75\sqrt{\pi}\, I \cdot t_a)^{2/3} \cdot \sigma \left[\frac{\varphi_i}{\rho\left(3CT_m + H_m + \frac{H_v}{\sqrt{27}}\right)} \right]^{2/3} \tag{2}$$

Here, k_w and F represent welding tendency and welding force, where higher k_w indicates better welding resistance. φ_a and φ_e are the work functions of the anode and the cathode material, respectively. T_m is the melting point, C is specific heat, λ is the thermal conductivity, and H_m and H_v are latent heat of fusion and vaporization, respectively.

Based on equations (1) and (2), higher ρ, T_m, C_P, H_m, H_v and λ values result in better welding resistance of electrical contact material. In this paper, compared with Cu, W has higher k_w and lower F values. Thus, with the W content increase from 25 wt% to 35 wt%, the welding force obviously decreased, i.e. welding resistance performance was enhanced.

4.2. Arc duration and energy

Arc duration and energy are important parameters. In addition, they have an important effect on arc erosion and mass change. The break arc duration of contact is affected by the contact material, vacuum degree, breaking speed, load and other factors [24–27]. Furthermore, arc duration also has a significant effect on arc energy. Fig. 12(a and b) shows the relationship between arc energy and arc duration of the two materials at 30 V DC, 30 A. It can be seen from the two curves, that a linear relationship exists between arc energy and arc duration. After fitting the data, the two equations are:

$$E_1 = 93.46t + 68.96 \quad R^2 = 0.97151 \tag{3}$$

$$E_2 = 105.54t\text{-}38.07 \quad R^2 = 0.963 \tag{4}$$

The corresponding (R^2) values for Eq. (3) and Eq. (4) are 0.97151 and 0.963, respectively. Fig. 12(c) shows the intersection of curves fitted using equations (3) and (4), which occurs at T_A = 8.86 ms. Thereafter, for the same arc energy, the arc duration of the 35 wt% W contact is shorter compared to 25 wt% W contact. For example, at points B and C, both materials have 3000 mJ arc energy, but the 25 wt% W composite undergoes T_C arc duration while the 35 wt% W composite undergoes T_B arc duration ($T_C > T_B$). Thus, the 35 wt% W composite exhibits better arc extinction performance.

5. Conclusion

(1) Vacuum hot-press sintering and internal oxidation were combined to fabricate the Al_2O_3-Cu/(W, Cr) composites. Dislocation tangles caused by the Al_2O_3 nano-particles pinning were clearly observed by the high resolution transmission electron microscope.

(2) After electrical contact test under 30 V DC and 10–30 A test conditions, the anodes of Al_2O_3-Cu/(25)W(5)Cr and Al_2O_3-Cu/(35)W(5)Cr electrical contact materials experienced an increase in mass, while the mass of the cathodes decreased. This indicates that the direction of material transfer was from the cathode to the anode.

(3) Gaseous arc erosion was the main erosion mechanism for the Al_2O_3-Cu/(25)W(5)Cr and Al2O3-Cu/(35)W(5)Cr composites. Liquid droplets, needle-like structures, craters, and bulges were formed on the electrode surfaces after arc erosion, and their quantity and morphology were affected by the tungsten content.

(4) The welding force of the electrical contacts decreased as dispersed W content increased, i.e. welding resistance improved with increasing W content. Compared with the 25 wt% W composite, the 35 wt% W composite experienced shorter arc duration at the same arc energy when the arc duration was longer than 8.86 ms. The welding resistance was also improved.

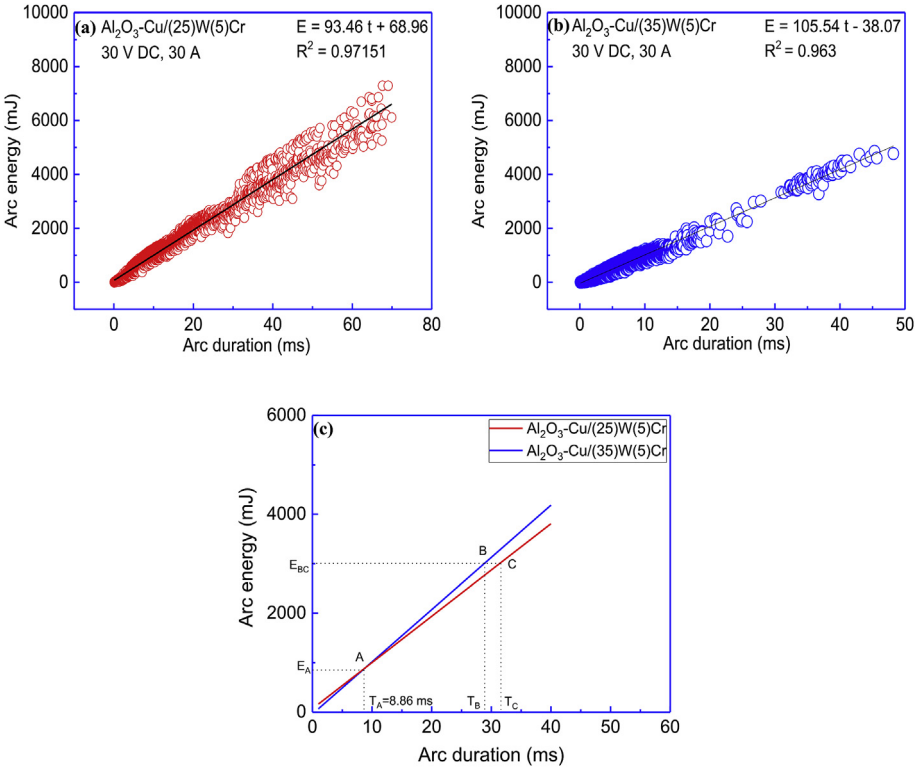

Fig. 12. Relationship between the arc energy and the arc duration of two materials at 30 V DC, 30 A: (a) Al_2O_3-Cu/(25)W(5)Cr; (b) Al_2O_3-Cu/(35)W(5)Cr; (c) the intersection of equations (3) and (4).

Acknowledgments

This work was supported by the Open Cooperation Project of Science and Technology of the Henan Province (172106000058), the Open Cooperation Project of Science and Technology of the Henan Province (182106000018), the Henan University Scientific and Technological Innovation Talent Support Program (18HASTIT024) and the National Natural Science Foundation of China (U1704143).

References

[1] Pons F. Electrical Contact Material Arc Erosion: Experiments and Modeling Towards the Design of an Silver Cadmium Oxide Substitute ProQuest Dissertations, and Theses Global 2010.
[2] Nachiketa R, Bernd K, Timo M, Ludo F, Kim V, Jef V. Effect of WC particle size and Ag volume fraction on electrical contact resistance and thermal conductivity of Ag-WC contact materials. Mater Des 2015;85:412–22.
[3] Zhen M, Geng HR, Li MM, Nie GL, Leng JF. Effects of Y_2O_3 on the property of copper based contact materials. Composites Part B 2013;52:51–5.
[4] Chen WG, Chen MZ, Xing LQ, Li JS, Hong F. Effect of doping on electrical arc characteristic of WCu electrical contact materials. Chin J Nonferrous Metals 2009;19:2029–3037.
[5] Saka K, Hasecawa M. Recent researches and new trends of electrical contacts. IEICE Trans Electron 2000;E83-C:1363–70.
[6] Tian BH, Liu P, Song KX, Li Y, Liu Y, Ren FZ, Su JH. Microstructure and properties at elevated temperature of a nano-$Al2O_3$ $_p$articles dispersion-strengthened copper base composite. Mater Sci Eng 2006;435–436:705–10.
[7] Bera S, Lojkowsky WM. Development of wear-resistant Cu-10Cr-3Ag electrical contacts with alloying and high pressure sintering. Metal Mat Trans A Phys Metall Mat Sci 2009;40:3276–83.
[8] Chang YL, Zheng W, Zhou ZM, Zhai YX, Wang YP. Preparation and performance of Cu-Cr contact materials for vacuum switches with low contact pressure. J Electron Mater 2016;45:5647–54.
[9] Yokokura K, Matsuda M, Atsumi K, Miyazawa T, Sohma S, Kaneko E, Ohshima I. Capacitor switching capability of vacuum interrupter with CuW Contact material. IEEE Trans Power Deliv 1995;10:804–9.
[10] Li Q, Ding M, Wu AP, Zou GS, Song W, Li J. Anti-welding performance of copper-based electrical contacts in solenoid switch. Chin J Nonferrous Metals 2013;23:2213–20.
[11] Nicolle C, Mazzucchi D, Gauthier JP, Gentils F. Behavior of CuCr and WCu contacts during making tests at high voltage and high currents. Proc Int Symp Discharge Electr Insul Vac ISDEIV 2010:261–4.
[12] Morris MA, Joye JC. Effect of the particle distribution on the mechanisms controlling deformation of a copper alloy at intermediate temperatures. Acta Metall Mater 1995;43:69–81.
[13] Scattergood RO, Koch CC, Murty KL, Brenner D. Strengthening mechanisms in nanocrystalline alloys. Mater Sci Eng 2008;1–2:3–11.
[14] Wang P, Gammer C, Brenne F, Niendorf T, Eckert J, Scudinoa S. A heat treatable TiB2/Al-3.5Cu-1.5Mg-1Si composite fabricated by selective laser melting: microstructure, heat treatment and mechanical properties. Composites Part B 2018;147:162–8.
[15] Mu Z, Geng HR, Li MM, Nie GL, Leng JF. Effects of Y_2O_3 on the property of copper based contact materials. Composites Part B 2013;52:51–5.
[16] Rong MZ, Yang ZY, Yang W. Contact material transfer of low voltage apparatus. Low Voltage Apparatus 1998;5:16–8.
[17] Chen ZK, SAWA K. Particle sputtering and deposition mechanism for material transfer in breaking arcs. J Appl Phys 1994;76:3326–31.
[18] Jemaa NB, Nedelec L, Benhenda S. Break arc duration and contact erosion in automotive application. IEEE Trans Compon Packag Manuf Technol 1996;19:82–6.
[19] Chen WG, Kang ZY, Shen HF, Ding BJ. Arc erosion behavior of a nanocomposite W-Cu electrical contact material. Rare Met 2006;25:37–42.
[20] Tepper J, Seeger M, Votteler T, Behrens V, Honig T. Investigation on erosion of Cu/W contacts in high-Voltage circuit breakers. IEEE Trans Compon Packag Technol 2006;29:658–65.
[21] Laurent M, Nouredine BJ, Didier J. Make arc erosion and welding in the automotive area. IEEE Trans Compon Packag Technol 2000;23:240–6.
[22] Yu L, Geng YS, Li Q, Wang JH, Liu ZY, Li DW, Wang WB, Wang XJ. Improvement of percussion welding characteristics of CuCr25 contact material by decreasing tensile strength. Proceedings of the 55th IEEE Holm Conference on Electrical Contacts. HOLM; 2009. p. 195–9.
[23] Liu XJ. Analysis of welding mechanism on electrical contact of switches. Low Voltage Apparatus 2006:11–4.
[24] Marcia E, Tom S. Low-voltage arc sustainability. IEEE IAS Electr Safe Workshop 2017;1.
[25] Niwa Y, Funahashi T, Yokokura K, Matsuzaki J, Homma M, Kaneko E. Basic investigation of a high-speed vacuum circuit breaker and its vacuum arc characteristics. IEE Proc Generat Transm Distrib 2006;153:11–5.
[26] Liang HM, Ma GC, Cai L, Xie Y, Xie GQ. Research on the relationship between contact breakaway initial velocity and arc duration. Electr Contacts Proc Annu Holm Conf Electr Contacts 2003:204–10.
[27] Chen ZK, Sawa K. Effect of oxide films and arc duration characteristics on Ag contact resistance behavior. IEEE Trans Compon Packag Manuf Technol 1995;18:409–16.